TSINGHUA SCIENCE AND TECHNOLOGY
ISSN 1007-0214 07/10 pp948–963
DOI: 10.26599/TST.2021.9010033
Volume 27, Number 6, December 2022

Observation-Driven Multiple UAV Coordinated Standoff Target Tracking Based on Model Predictive Control

Shun Sun, Yu Liu*, Shaojun Guo*, Gang Li, and Xiaohu Yuan

Abstract: An observation-driven method for coordinated standoff target tracking based on Model Predictive Control (MPC) is proposed to improve observation of multiple Unmanned Aerial Vehicles (UAVs) while approaching or loitering over a target. After acquiring a fusion estimate of the target state, each UAV locally measures the observation capability of the entire UAV system with the Fisher Information Matrix (FIM) determinant in the decentralized architecture. To facilitate observation optimization, only the FIM determinant is adopted to derive the performance function and control constraints for coordinated standoff tracking. Additionally, a modified iterative scheme is introduced to improve the iterative efficiency, and a consistent circular direction control is established to maintain long-term observation performance when the UAV approaches its target. Sufficient experiments with simulated and real trajectories validate that the proposed method can improve observation of the UAV system for target tracking and adaptively optimize UAV trajectories according to sensor performance and UAV-target geometry.

Key words: coordinated tracking; standoff tracking; observation-driven; Model Predictive Control (MPC); multiple UAVs; Fisher Information Matrix (FIM)

1 Introduction

Cooperative target tracking has emerged as a topic of interest to the information fusion and control community[1]. When a fixed-wing Unmanned Aerial Vehicle (UAV) continuously tracks a target at economical cruising speed, it should maintain a distance from the target to ensure continuous, persistent, efficient situation awareness and safety of the UAV itself. This strategy introduces standoff target tracking, especially for the coordinate tracking of multiple UAVs.

Methods based on Lyapunov Vector Field Guidance (LVFG)[2–4] are globally stable and easily implemented onboard. By decoupling the heading control and the speed control, LVFG-based methods achieve stable standoff tracking and phase keeping[5–7]. Alternatively, methods based on Model Predictive Control (MPC)[8, 9] can yield optimal control to minimize an objective function and are further developed for standoff target tracking. For example, tracking control of ground moving targets was achieved using a single fixed-wing UAV[10]. A performance function is constructed to describe standoff distance and phase constraints between two UAVs and the target, and nonlinear MPC was employed for coordinated standoff tracking[11].

• Shun Sun is with the Department of Control Science and Technology, Naval Aviation University, Yantai 264001, China. E-mail: sunms7@qq.com.
• Yu Liu is with the Department of Control Science and Technology, Naval Aviation University, Yantai 264001, China, and also with the Department of Electronic Engineering, Tsinghua University, Beijing 100084, China. E-mail: liuyu77360132@126.com.
• Shaojun Guo is with National Institute of Defense Technology Innovation, Academy of Military Sciences PLA, Beijing 100091, China. E-mail: guoba2000@163.com.
• Gang Li is with the Department of Electronic Engineering, Tsinghua University, Beijing 100084, China. E-mail: gangli@mail.tsinghua.edu.cn.
• Xiaohu Yuan is with Department of Automation, Tsinghua University, Beijing 100084, China. E-mail: yuanxh8@tsinghua.edu.cn.
∗ To whom correspondence should be addressed.
Manuscript received: 2021-03-09; revised: 2021-04-20; accepted: 2021-04-22

However, the above methods ignore the effect of sensor performance and geometry between multiple UAVs on the observation performance for target tracking, regardless of whether the UAVs approach the target or steady hover on the circular orbit.

To determine the effect of the UAV geometry and sensor performance on the observation capability, some indices such as the Cramér-Rao Lower Bound (CRLB)[12], Fisher Information Matrix (FIM)[13–15], target state estimated covariance[16], and related variants[17], are used to measure the target observation capability during tracking. According to accuracy analysis with two UAVs[18], the bearing measurements require a 90° line-of-sight angle between the two UAVs and target, and the distance between the UAV and target should be a minimum, which is equal to the standoff radius in the standoff tracking. The radial distance measurement only requires the angle between the sightline of UAVs to be 90°, which is insensitive to the target-UAV distance. Therefore, the optimal position distribution of two UAVs measuring both bearing and distance is that UAVs fly on the standoff circle, and their phase difference is 90°. Bishop et al.[19] further provided the optimal geometries for more UAVs. Therefore, optimal target observation requires consideration of the sensor accuracy and the geometry between UAVs for a coordinated standoff tracking system. By introducing accuracy analysis to existing multiple UAV coordinated standoff tracking based on LVFG or MPC, the observation of the UAVs can be improved and close to optimum, only on the loitering orbit. However, because these methods rely on prior analysis under specified parameters, their adaptability to the number of UAVs is limited, especially for those equipped with asymmetric sensors.

When the target position is unknown, or the UAVs follow a high-speed target, a team of UAVs commonly approaches the target from a long distance. However, the UAVs cannot achieve optimal UAV-target configuration in a short time, and static accuracy analysis cannot guide the observation improvement with saturation input of UAV either. Therefore, it is critical to find a way to quickly improve observation within the limited maneuverability of UAVs in coordinated tracking.

To address these problems and limitations, the observation capability of the UAVs system can be used to structure the objective function for closed-loop control optimization. To this end, standoff tracking and collision avoidance can be achieved using potential fields[16], and gradient-based control law can be used to iteratively solve the control problem. However, this approach is similar to a single-step search, and the resulting trajectories lack prediction. Additionally, the MPC-based optimal cooperative reconnaissance method[20] uses the summary of weighted cost functions to describe target information, high-risk zones, and vehicle constraints. However, it is the same as other MPC-based methods[11] in which the weighted penalty/cost functions are used to constrain the UAV behavior, and the expression of UAV observation performance is distorted. Consequently, the optimal observation improvement of UAVs cannot be guaranteed when they fly to the target.

Inspired by an end-to-end concept and MPC-based methods, the FIM determinant is used as a computable observation metric of multiple UAVs to drive UAV trajectory optimization for improving coordinated tracking. In this study, an observation-driven MPC-based method is proposed to significantly improve the observation capability for standoff target tracking using multiple fixed-wing UAVs. The optimal control of each UAV can be determined according to the sensor performance and UAV-target geometry in the decentralized architecture, where optimal control means the fastest improvement observation of the UAV system for target localization and tracking. To facilitate observation optimization, only the determinant of the FIM is used to derive the performance function and control constraints for coordinated standoff tracking. Moreover, a modified iterative scheme is introduced to improve the iterative efficiency, and a consistent circular direction control is established to maintain long-term observation performance when the UAV approaches its target. Simulated and semi-simulated experiments are used to verify the performance of the proposed method.

The main contributions of this method can be summarized as follows:

- The determinant of the FIM is adopted to measure the observation of the UAV system with a local fuzed target state estimate. In the decentralized architecture, a novel performance function based on FIM for coordinated standoff tracking is derived, which quickly drives UAV trajectories to an observation improvement.
- A constraint scheme is introduced to describe the saturation of UAV control commands. The scheme avoids the impact of weighted penalty functions on control optimization direction for standoff tracking.
- The gradient in the control optimization step is reconstructed with normalization and sign functions

to improve iterative efficiency. A new termination criterion for iteration and an iterative initialization for the control sequence are presented to ensure the control accuracy and improve the computational efficiency of the optimization process. Additionally, the inconsistent motion direction of UAVs on the standoff circle is corrected to break the limit of the MPC-based method for long-term prediction.

• Two UAV situations with different measurement errors and initial distances indicate the proposed method is adaptive to approach optimal observation. Experiments with different UAVs illustrate the scalability of the proposed method. Semi-simulations using a real ground vehicle trajectory in GeoLife are followed to further verify effectiveness and efficiency.

The remainder of this paper is organized as follows. Section 2 describes the coordinated standoff tracking problem, UAV kinematic model, and target state estimation. Section 3 details the proposed method and its iterative solution in the decentralized architecture. Improved optimization schemes and consistent circular direction control are presented in Section 4. Sufficient simulations and analysis in Section 5 demonstrate the effectiveness and advantages of the proposed algorithm. Finally, conclusions are summarized in Section 6.

2 Problem Statement

Multiple UAV collaboration can enhance the continuity of standoff target tracking and situational awareness. Assume that multiple UAVs fly at a fixed altitude on a plane. To ensure safety and an adequate field of view, standoff tracking requires the UAVs to maintain a constant distance from the target. In addition, the UAV team aims to maintain angular separation to obtain more comprehensive information on the target or environment.

2.1 UAV kinematic model

The kinematic model of a UAV can be established as follows:

$$\begin{bmatrix} \dot{x}_k \\ \dot{y}_k \\ \dot{\varphi}_k \\ \dot{v}_k \\ \dot{\omega}_k \end{bmatrix} = \boldsymbol{f}_d(\boldsymbol{x}_k, \boldsymbol{u}_k) = \begin{bmatrix} v_k \cos\varphi_k \\ v_k \sin\varphi_k \\ \omega_k \\ \frac{1}{\tau_v}(u_{v,k} - v_k) \\ \frac{1}{\tau_\omega}(u_{\omega,k} - w_k) \end{bmatrix} \tag{1}$$

where $\boldsymbol{x}_k = [x_k, y_k, \varphi_k, v_k, \omega_k]^{\mathrm{T}}$ are the inertial position, heading, speed, and yaw rate of the UAV, respectively, and τ_v and τ_ω are time constants for considering actuator delay. The UAV state update equation is $\boldsymbol{x}_{k+1} = \boldsymbol{f}_k = \boldsymbol{x}_k + T_s \boldsymbol{f}_d(\boldsymbol{x}_k, \boldsymbol{u}_k)$, and T_s denotes a sensor sampling time. Vector $\boldsymbol{u}_k = [u_{v,k}, u_{\omega,k}]^{\mathrm{T}}$ represents the speed and turning rate commands constrained by

$$\left|u_{v,k} - v_0\right| \leqslant \Delta v_{\max} \tag{2}$$

$$\left|u_{\omega,k}\right| \leqslant \omega_{\max} \tag{3}$$

where v_0 is a nominal speed of UAV, and $\Delta v_{\max}$ and $w_{\max}$ are the maximum speed change and turning rate of UAV, respectively.

2.2 Target state estimation

Assume multiple UAVs perform coordinated standoff moving target tracking. Each UAV can sense the target and collect bearing and radial distance measurements to locate the target based on extended Kalman filter[21], where the corresponding measurement functions can be defined as

$$\boldsymbol{h}(\boldsymbol{x}_{t,k}, \boldsymbol{x}_{i,k}) = \begin{bmatrix} \rho_{i,k} \\ \beta_{i,k} \end{bmatrix} = \begin{bmatrix} \|\boldsymbol{x}_{t,k} - \boldsymbol{x}_{i,k}\| \\ \arctan\frac{y_{t,k} - y_{i,k}}{x_{t,k} - x_{i,k}} \end{bmatrix} \tag{4}$$

where $\boldsymbol{x}_{t,k}$ and $\boldsymbol{x}_{i,k}$ are the position state of the target and UAV i, respectively.

The target state estimate results of each UAV can be transmitted to each other via communication links. When a UAV receives the estimates from its neighbors, the estimation accuracy can be improved by fuzing estimations from different UAVs via suboptimal distributed fusion[21], fusion rule based on Kullback-Leibler divergence[22], or cooperative target tracking in wireless sensor networks[23, 24]. In this paper, the fuzed target state estimate with respect to UAV i is given as

$$\boldsymbol{x}_{Fi,k} = \boldsymbol{P}_{Fi,k}\left(\sum_{j\in N} \boldsymbol{P}_{j,k}^{-1}\boldsymbol{x}_{tj,k}\right) \tag{5}$$

$$\boldsymbol{P}_{Fi,k} = \left(\sum_{j\in N} \boldsymbol{P}_{j,k}^{-1}\right)^{-1} \tag{6}$$

where N is the set of UAVs, and $\boldsymbol{x}_{tj,k}$ and $\boldsymbol{P}_{j,k}$ are the target position state estimate and its error covariance of UAV j, respectively.

The specific scenario schematic diagram of the target state estimation and fusion for multiple UAV coordinated standoff tracking is presented in Fig. 1.

3 Observation-Driven Coordinated Standoff Tracking

3.1 Performance function

The observation capability of the UAV tracking system for a target is affected by the measurement

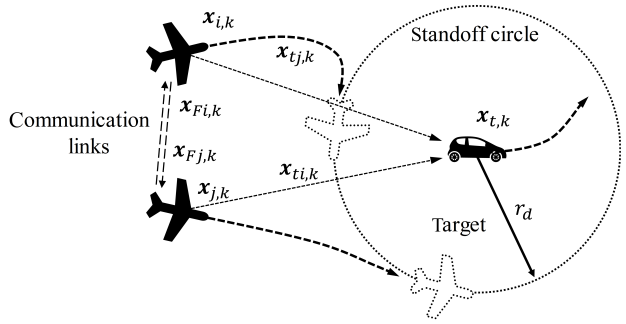

Fig. 1 Specific scenario schematic diagram, where two UAVs perform coordinated standoff tracking, estimate the target state based on an extended Kalman filter locally, and then improve the estimation accuracy with distributed fusion via communication links.

type, random measurement error, and the geometry between multiple UAVs and the target. The FIM[13–15], CRLB[12], localization error covariance matrix[16], and related variants[17] can be used to describe the effect of observation capability on target localization and tracking. As the prediction of localization error covariance requires intermediate results in the tracking filter, it increases the communication burden between UAVs. The CRLB is equal to the inverse of the FIM and denotes the minimum variance of the unbiased estimator; therefore, FIM is a metric to measure the observation performance and avoids the inverse operation. Trace, determinant, and maximum eigenvalue are usually used as scalar evaluations of the FIM. The maximum eigenvalue may lose secondary information corresponding to the non-maximum eigenvalue, and the calculation of its derivative is not concise. For the trace of FIM, the sum of the matrix traces is equal to the trace of the sum of the matrices. If we take the derivative of the amount of FIMs with respect to the UAV state, the effect of the other UAVs on the observation is ignored. The determinant of the FIM is inversely proportional to the uncertainty area of the estimator and characterizes the nature of the likelihood function of the target position state given the measurement. Therefore, the FIM is an available scalar functional measure of the observation capability for the multiple UAV system.

In a decentralized sensor network composed of UAVs, each UAV can obtain the target state estimate and the corresponding error covariance, and predict control sequences of other UAVs via communication links. Each UAV can then fuze state estimation of the target with high accuracy and measure the observation performance of the UAV system. FIM $\boldsymbol{M}_{i,k}$ of UAV i for the target at time k can be expressed as

$$\boldsymbol{M}_{i,k}=\boldsymbol{H}_{x_{t,k}}^{\mathrm{T}}\boldsymbol{R}_{i,k}^{-1}\boldsymbol{H}_{x_{t,k}} \tag{7}$$

where $\boldsymbol{x}_{t,k}$ is the UAV position estimated based on GPS or inertial measurement unit, $\boldsymbol{H}_{x_{t,k}}$ is the Jacobian matrix of measurement equations $\boldsymbol{h}(\boldsymbol{x}_{t,k},\boldsymbol{x}_{i,k})$ with respect to the target position state $\boldsymbol{x}_{t,k}$, and $\boldsymbol{R}_{i,k}$ is the measurement covariance of the sensor on UAV i. As the true position of the target is unknown, the fuzed target state $\boldsymbol{x}_{Fi,k}$ of each UAV substitutes $\boldsymbol{x}_{t,k}$ for algorithm execution.

The aim is to improve observation of multiple UAVs for the target by minimizing a performance function that accounts for the effect of sensor performance and geometry between the UAVs and the target. Therefore, the negative determinant of the sum of the FIM for all UAVs is adopted as the performance metric,

$$L_{i,k}=-\left|\sum_{j\in N}\boldsymbol{M}_{j,k}\right|,\ \left\|\boldsymbol{x}_{Fi,k}-\boldsymbol{x}_{i,k}\right\|\geqslant r_d \tag{8}$$

where r_d is the standoff distance.

The above metric only measures the current observation of the UAV system. The actual observation capability is difficult to measure during the whole tracking process, because the real target state, dynamic model, and its process noise are unknown, disturbance from background wind is time-varying, and UAV self-positioning contains errors. However, the performance metric in Eq. (8) can approximatively predict the greatest change in observation performance at a future moment using state extrapolations based on predefined dynamic models. If the UAVs move according to the greatest observation increment at each time step, the UAV system obtains approximated optimal observation during the entire tracking process.

Furthermore, to maintain a predefined distance between each UAV and the target for coordinated tracking (i.e., to maintain UAVs outside the standoff circle), when UAV i is inside the standoff circle, the determinant of its FIM is selected as the performance metric,

$$L_{i,k}=\left|\boldsymbol{M}_{i,k}\right|,\ \left\|\boldsymbol{x}_{Fi,k}-\boldsymbol{x}_{i,k}\right\|<r_d \tag{9}$$

Along with a receding horizon control with respect to UAV i, the performance function driven by the UAVs observation in the decentralized architecture is given by

$$J_i=\sum_{l=k}^{k+N_r}L_{i,l} \tag{10}$$

where N_r is the receding horizon length.

The design of Eq. (10) considers two main aspects.

A penalty function with minimum values on the

standoff circle is usually added to the performance function to achieve loitering movement, such as the Lyapunov function in LVFG[16]. A choreographed weight is required to adjust the magnitude of the penalty function, limiting generalizability and applicability. If the value of the weighted penalty function is large, the many iterations may slow the convergence and even lead to divergence. Otherwise, the constraints from penalty functions may not be reflected in the solution. The proposed performance function designed with piecewise can improve coordinated observation of multiple UAVs in the loitering pattern whether the UAV is inside or outside the standoff circle.

Alternatively, the determinant of the FIM is inversely proportional to the squared distance from the UAV to the target for radar sensors. Therefore, the performance function value varies over a large range for different performances of sensors installed on the UAVs and different parameters in standoff tracking for different targets or mission types. When control commands are optimized near the standoff circle by minimizing the performance function in Eq. (10), the absolute values of the performance function derivative have a similar magnitude. Therefore, control commands can be optimized radially away from the target when the UAV is inside the standoff circle. The above features of the established performance function can avoid incorrect optimization directions for UAV coordination and improve the efficiency of iterative optimization. Additionally, the features also contribute to the generalizability of standoff tracking.

A similar strategy for iterative optimization is adopted to handle saturation constraints of the UAV control input. According to Eqs. (2) and (3), the penalty functions for the control constraints are expressed as

$$\boldsymbol{g}(\boldsymbol{u}_{i,k}) = \begin{bmatrix} g_v(u_{vi,k}) \\ g_\omega(u_{\omega i,k}) \end{bmatrix} \leqslant 0 \tag{11}$$

The coordinated standoff tracking control driven by observation can then be constructed as a nonlinear optimal control problem that minimizes the objective function under constraints,

$$\boldsymbol{U}^*_{i,k} = \underset{\boldsymbol{U}_{i,k}}{\arg\min}\, J_i, i \in N \tag{12}$$

subject to

$$\boldsymbol{f}_{i,k} - \boldsymbol{x}_{i,k+1} = 0 \tag{13}$$

$$\boldsymbol{g}(\boldsymbol{u}_{i,k}) \leqslant 0 \tag{14}$$

where $\boldsymbol{U}^*_{i,k} = \{\boldsymbol{u}^*_{i,l}, l = k, \ldots, k+N_r-1\}$ is the optimal control sequence for UAV i.

Incorporating the UAV kinematic model and inequality constraints of saturation, an augmented performance function can be expressed as follows:

$$J_{a,i} = \sum_{l=k}^{k+N_r} L_{i,l} + \sum_{l=k}^{k+N_r-1} \{\boldsymbol{\lambda}^{\mathrm{T}}_{l+1}(\boldsymbol{f}_{i,l} - \boldsymbol{x}_{i,l+1}) + \boldsymbol{\mu}^{\mathrm{T}}_l \boldsymbol{g}(\boldsymbol{u}_{i,l})\} = L_{i,k+N_r} + \sum_{l=k}^{k+N_r-1} \{H_{i,l} - \boldsymbol{\lambda}^{\mathrm{T}}_{l+1}\boldsymbol{x}_{i,l+1}\}, i \in N \tag{15}$$

$$H_{i,l} = L_{i,l} + \boldsymbol{\lambda}^{\mathrm{T}}_{l+1}\boldsymbol{f}_{i,l} + \boldsymbol{\mu}^{\mathrm{T}}_l \boldsymbol{g}(\boldsymbol{u}_{i,l}), l = k, \ldots, k+N_r-1 \tag{16}$$

where $H_{i,l}$ is the following Hamiltonian function, $\boldsymbol{\lambda}_{l+1} \in \mathbf{R}_{5\times 1}$ is a Lagrangian multiplier, and $\boldsymbol{\mu}_l \in \mathbf{R}^+_{2\times 1}$ is a weight vector of positive real numbers. The optimization problem in Eq. (12) can be transformed into

$$\boldsymbol{U}^*_{i,k} = \underset{\boldsymbol{U}_{i,k}}{\arg\min} \sum_{l=k}^{k+N_r-1} H_{i,l}, \quad i \in N \tag{17}$$

3.2 Solution to optimal control

The variation of the augmented performance function in Eq. (15) yields

$$\begin{aligned} \mathrm{d}J_{a,i} = {} & \frac{\partial L_{i,k+N_r}}{\partial \boldsymbol{x}_{i,k+N_r}}\mathrm{d}\boldsymbol{x}_{i,k+N_r} + \\ & \sum_{l=k}^{k+N_r-1}\left[\frac{\partial H_{i,l}}{\partial \boldsymbol{x}_{i,l}}\mathrm{d}\boldsymbol{x}_{i,l} + \frac{\partial H_{i,l}}{\partial \boldsymbol{u}_{i,l}}\mathrm{d}\boldsymbol{u}_{i,l} - \boldsymbol{\lambda}^{\mathrm{T}}_{l+1}\mathrm{d}\boldsymbol{x}_{i,l+1}\right] = \\ & \left[\frac{\partial L_{i,k+N_r}}{\partial \boldsymbol{x}_{i,k+N_r}} - \boldsymbol{\lambda}^{\mathrm{T}}_{k+N_r}\right]\mathrm{d}\boldsymbol{x}_{i,k+N_r} + \\ & \sum_{l=k+1}^{k+N_r-1}\left\{\left[\frac{\partial H_{i,l}}{\partial \boldsymbol{x}_{i,l}} - \boldsymbol{\lambda}^{\mathrm{T}}_l\right]\mathrm{d}\boldsymbol{x}_{i,l} + \frac{\partial H_{i,l}}{\partial \boldsymbol{u}_{i,l}}\mathrm{d}\boldsymbol{u}_{i,l}\right\} + \\ & \frac{\partial H_{i,k}}{\partial \boldsymbol{x}_{i,k}}\mathrm{d}\boldsymbol{x}_{i,k} + \frac{\partial H_{i,k}}{\partial \boldsymbol{u}_{i,k}}\mathrm{d}\boldsymbol{u}_{i,k} \end{aligned} \tag{18}$$

Let the Lagrange multiplier be

$$\boldsymbol{\lambda}^{\mathrm{T}}_{k+N_r} = \frac{\partial L_{i,k+N_r}}{\partial \boldsymbol{x}_{i,k+N_r}} \tag{19}$$

$$\boldsymbol{\lambda}^{\mathrm{T}}_l = \frac{\partial H_{i,l}}{\partial \boldsymbol{x}_{i,l}}, l = k+N_r-1, \ldots, k+1 \tag{20}$$

The variation of the augmented performance function is

$$\mathrm{d}J_{a,i} = \sum_{l=k}^{k+N_r-1}\left\{\frac{\partial H_{i,l}}{\partial \boldsymbol{u}_{i,l}}\mathrm{d}\boldsymbol{u}_{i,l}\right\} + \frac{\partial H_{i,k}}{\partial \boldsymbol{x}_{i,k}}\mathrm{d}\boldsymbol{x}_{i,k} \tag{21}$$

where

$$\frac{\partial H_{i,l}}{\partial \boldsymbol{x}_{i,l}} = \frac{\partial L_{i,l}}{\partial \boldsymbol{x}_{i,l}} + \boldsymbol{\lambda}^{\mathrm{T}}_{l+1}\frac{\partial \boldsymbol{f}_{i,l}}{\partial \boldsymbol{x}_{i,l}} \tag{22}$$

$$\frac{\partial \boldsymbol{f}_{i,l}}{\partial \boldsymbol{x}_{i,l}} = \begin{bmatrix} 1 & 0 & -v_{i,l}\sin\varphi_{i,l}T_s & \cos\varphi_{i,l}T_s & 0 \\ 0 & 1 & v_{i,l}\cos\varphi_{i,l}T_s & \sin\varphi_{i,l}T_s & 0 \\ 0 & 0 & 1 & 0 & T_s \\ 0 & 0 & 0 & 1-\dfrac{T_s}{\tau_v} & 0 \\ 0 & 0 & 0 & 0 & 1-\dfrac{T_s}{\tau_\omega} \end{bmatrix} \tag{23}$$

When $\left\|\boldsymbol{x}_{Fi,l} - \hat{\boldsymbol{x}}_{t,l}\right\| \geqslant r_d$, by substituting Eq. (8), we obtain $\dfrac{\partial L_{i,l}}{\partial \boldsymbol{x}_{i,l}}$ as follows:

$$\frac{\partial L_{i,l}}{\partial \boldsymbol{x}_{i,l}} = -2\left|\sum_{j\in N}\boldsymbol{M}_{j,l}\right| \operatorname{vec}\left(\boldsymbol{R}_{i,l}^{-1}\boldsymbol{H}_{\boldsymbol{x}_{t,l}}\left(\sum_{j\in N}\boldsymbol{M}_{j,l}\right)^{-1}\right)^{\mathrm{T}} \frac{\partial \operatorname{vec}(\boldsymbol{H}_{\boldsymbol{x}_{t,l}})}{\partial \boldsymbol{x}_{i,l}^{\mathrm{T}}} \tag{24}$$

$$\boldsymbol{H}_{\boldsymbol{x}_{t,k}} = \frac{\partial \boldsymbol{h}(\boldsymbol{x}_{t,k}, \boldsymbol{x}_{i,k})}{\partial \boldsymbol{x}_{t,k}^{\mathrm{T}}} = \begin{bmatrix} \dfrac{x_{t,k}-x_{i,k}}{\rho_{i,k}} & \dfrac{y_{t,k}-y_{i,k}}{\rho_{i,k}} \\ -\dfrac{y_{t,k}-y_{i,k}}{\rho_{i,k}^2} & \dfrac{x_{t,k}-x_{i,k}}{\rho_{i,k}^2} \end{bmatrix} \tag{25}$$

$$\frac{\partial \operatorname{vec}(\boldsymbol{H}_{\boldsymbol{x}_{t,k}})}{\partial \boldsymbol{x}_{i,k}^{\mathrm{T}}} = \frac{1}{\rho_{i,k}^4} \times \begin{bmatrix} -(y_{i,k}-y_{t,k})^2\rho_{i,k} & (x_{i,k}-x_{t,k})(y_{i,k}-y_{t,k})\rho_{i,k} \\ -2(x_{i,k}-x_{t,k})(y_{i,k}-y_{t,k}) & (x_{i,k}-x_{t,k})^2-(y_{i,k}-y_{t,k})^2 \\ (x_{i,k}-x_{t,k})(y_{i,k}-y_{t,k})\rho_{i,k} & -(x_{i,k}-x_{t,k})^2\rho_{i,k} \\ (x_{i,k}-x_{t,k})^2-(y_{i,k}-y_{t,k})^2 & 2(x_{i,k}-x_{t,k})(y_{i,k}-y_{t,k}) \end{bmatrix} \tag{26}$$

where $\operatorname{vec}(\cdot)$ represents column stacking vectorization and $\boldsymbol{R}_{i,l}^{-1}$ is a real symmetric matrix.

Similarly, when $\|\boldsymbol{x}_{Fi,l} - \hat{\boldsymbol{x}}_{t,l}\| < r_d$, we have

$$\frac{\partial L_{i,l}}{\partial \boldsymbol{x}_{i,l}} = 2\left|\boldsymbol{M}_{i,l}\right| \operatorname{vec}\left(\boldsymbol{R}_{i,l}^{-1}\boldsymbol{H}_{\boldsymbol{x}_{t,l}}\boldsymbol{M}_{i,l}^{-1}\right)^{\mathrm{T}} \frac{\partial \operatorname{vec}(\boldsymbol{H}_{\boldsymbol{x}_{t,l}})}{\partial \boldsymbol{x}_{i,l}} \tag{27}$$

A gradient descent method can be iteratively applied to optimize control commands by minimizing the Hamiltonian function as follows:

$$\boldsymbol{u}_{i,l}^{t+1} = \boldsymbol{u}_{i,l}^{t} - \Delta_{i,l}^{t}\frac{\partial H_{i,l}^{\mathrm{T}}}{\partial \boldsymbol{u}_{i,l}}, l = k, \ldots, k+N_r-1 \tag{28}$$

$$\frac{\partial H_{i,l}^{\mathrm{T}}}{\partial \boldsymbol{u}_{i,l}} = \boldsymbol{\lambda}_{l+1}^{\mathrm{T}}\frac{\partial \boldsymbol{f}_{i,l}}{\partial \boldsymbol{u}_{i,l}} + \boldsymbol{\mu}_k^{\mathrm{T}}\frac{\partial \boldsymbol{g}(\boldsymbol{u}_{i,l})}{\partial \boldsymbol{u}_{i,l}} \tag{29}$$

where t is the iteration number and $\Delta_{i,l}^{t}$ is the step length of the iteration.

The variation of the augmented performance function becomes

$$\mathrm{d}J_{a,i} = -\sum_{l=k}^{k+N_r-1}\left\{\Delta_{i,l}^{t}\frac{\partial H_{i,l}}{\partial \boldsymbol{u}_{i,l}}\frac{\partial H_{i,l}^{\mathrm{T}}}{\partial \boldsymbol{u}_{i,l}}\right\} + \frac{\partial H_{i,k}}{\partial \boldsymbol{x}_{i,k}}\mathrm{d}\boldsymbol{x}_{i,k} \tag{30}$$

The saturation constraints of the UAV are generally expressed as a switching penalty function. When a control term satisfies the saturation constraint, its penalty function is set as zero; otherwise, the penalty function performs a suppression effect on the performance function with a positive value. The design of a penalty function and its weight are also sensitive to control scenarios; hence, a strategy similar to that in Eqs. (8) and (9) is applied. When the control satisfies the saturation constraint $\boldsymbol{\lambda}_{l+1}^{\mathrm{T}}\dfrac{\partial \boldsymbol{f}_{i,l}}{\partial \boldsymbol{u}_{i,l}}$. Otherwise, the optimization direction for control is reversed. The calculation of $\dfrac{\partial H_{i,l}^{\mathrm{T}}}{\partial \boldsymbol{u}_{i,l}}$ can be modified with sign functions as

$$\frac{\partial H_{i,l}^{\mathrm{T}}}{\partial \boldsymbol{u}_{i,l}} = \boldsymbol{\lambda}_{l+1}^{\mathrm{T}}\frac{\partial \boldsymbol{f}_{i,l}}{\partial \boldsymbol{u}_{i,l}}\begin{bmatrix} g_v^*(u_{vi,l}) & 0 \\ 0 & g_\omega^*(u_{\omega i,l}) \end{bmatrix} \tag{31}$$

$$g_v^*(u_{vi,l}) = \operatorname{sign}\left(\Delta v_{i,\max} - \left|u_{vi,l} - v_c\right|\right) \tag{32}$$

$$g_\omega^*(u_{\omega i,l}) = \operatorname{sign}(\omega_{i,\max} - \left|u_{\omega i,l}\right|) \tag{33}$$

4 Improved Optimization and Circular Direction Control

After obtaining the gradient direction of control commands using Eq. (31), the control sequence can be obtained by the iterative method with appropriate step length to make the performance function continuously decrease. As a result, the observation of the UAV system can be improved in the optimal direction. Some improved optimization schemes and consistent circular direction control are presented.

4.1 Gradient normalization

Each element in the negative gradient direction $-\dfrac{\partial H_{i,l}^{\mathrm{T}}}{\partial \boldsymbol{u}_{i,l}}$ represents an optimization direction of the performance function for the corresponding control command. Therefore, on the same scale, different magnitudes indicate the contributions of different control commands to the observation improvement. However, as control inputs $u_{vi,l}$ and $u_{\omega i,l}$ are independent and have different ranges for UAV i, the direction (positive or negative) of each element in the gradient vector is more important than its absolute value for control optimization. Therefore, normalization and sign

functions are introduced and the iterative optimization step in Eq. (28) is updated as

$$\boldsymbol{u}_{i,l}^{t+1} = \boldsymbol{u}_{i,l}^{t} - \Delta_{i,l}^{t}\mathrm{diag}(\boldsymbol{\eta}_i)\mathrm{sign}\left(\frac{\partial H_{i,l}^{\mathrm{T}}}{\partial \boldsymbol{u}_{i,l}}\right) \tag{34}$$

where the normalization factor $\boldsymbol{\eta}_i = \left[\dfrac{\Delta v_{i,\max}}{\omega_{i,\max}}, 1\right]$.

4.2 Termination criterion

In existing MPC-based methods, when the performance function varies less than a threshold, the iterative process terminates, ensuring acceptable optimization accuracy. However, this is not available for the proposed method, whose performance function exhibits discontinuity points on the standoff circle. When a UAV is close to the standoff circle, the performance function changes greatly, impeding algorithm termination using the threshold criterion. Instead, the iteration step length is selected as a termination criterion. When the performance function increases rather than decreases in the iterative step, the step length decreases, and a sufficiently small length indicates a low optimization effect on control. Thus, it is appropriate to terminate the algorithm when a small step length is reached.

4.3 Iterative initialization of the control sequence

Before executing the proposed algorithm, the control sequence is initialized as

$$\boldsymbol{U}_i^0 = \{\boldsymbol{u}_{i,l}^0, l = k, \ldots, k + N_r - 1\} \tag{35}$$

where the value of the control command is initialized as $\boldsymbol{u}_{i,l}^0 = [v_c, 0]^{\mathrm{T}}$. Notice that the initialization of the turning rate with 0 ensures that the motion direction of the UAVs on the standoff circle is not predefined, but adaptively selected to improve the observation performance. If the current control sequence after optimization is $\boldsymbol{U}_{i,k}^* = \{\boldsymbol{u}_{i,k}^*, \boldsymbol{u}_{i,k+1}^*, \ldots, \boldsymbol{u}_{i,k+N_r-1}^*\}$, the control sequence in the next time step is iteratively initialized as $\boldsymbol{U}_{i,k+1}^0 = \{\boldsymbol{u}_{i,k+1}^*, \ldots, \boldsymbol{u}_{i,k+N_r-1}^*, \boldsymbol{u}_{i,k+N_r-1}^*\}$.

4.4 Consistent circular direction control

The MPC-based method has poor results on long-term control because of the limited record horizon length. For the proposed method, when the UAV is close to the standoff circle, its motion direction is determined only according to the observation performance of the record horizon. However, if the circular direction of the UAVs is inconsistent, their phase separation will periodically vary, as well as the observation capability of the UAVs system because of maintaining the standoff distance. Therefore, when the UAV is close enough to the circular orbit, its tangential velocity relative to the target should be consistent with the first UAV that hovers on the standoff orbit or a manual setup in advance. Detection of the circular direction is triggered when the distance between the UAV and target is less than r_{thres}, where r_{thres}=$r_d + r_{turn}$, and r_{turn} is the turning radius at the current speed. If the circular direction is inconsistent with other UAVs or a manual setup, the LVFG-based method is used to calculate the turning rate command at the current moment, where the direction of the vector field should agree with the desired circular direction. Concurrently, the turning rate commands in the control sequence are initialized as 0, except the current moment and the speed commands remain unchanged.

Through communication, each UAV can mutually transfer the motion state, sensor performance, observation for the target, and the control sequence of the UAV at the last moment. The distributed state estimate can then be used to fuze multiple measurements and improve the estimation accuracy of the target state. Each UAV optimizes the control sequence using the above information in the decentralized architecture. In the process of the control sequence iteration, there is no communication among the UAVs, so the proposed method can effectively reduce the communication burden, and it is easy for engineering practice. The specific multiple UAV coordinated tracking system architecture is present in Fig. 2.

The algorithm flow is illustrated in Algorithm 1 to state the proposed method more clearly.

5 Simulation Experiments and Analysis

The performance of the proposed method is presented and verified with a ground vehicle target trajectory. Multiple UAVs are used to perform the standoff target tracking mission. Initially, the first UAV position is initialized at (0, 0) m, and the other UAVs line up west with an interval of 100 m. All of the UAV head 0° to the

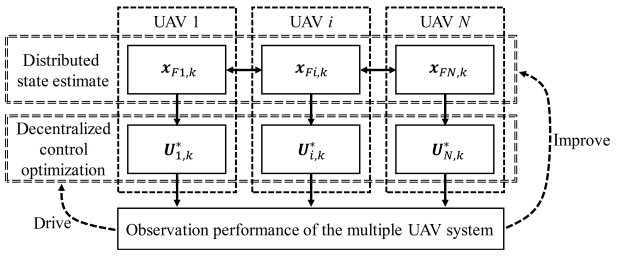

Fig. 2 Multiple UAV coordinated tracking system architecture.

Algorithm 1 Proposed method for UAV i at time k

Input: Fuzed target state estimate $\boldsymbol{x}_{Fi,k}$, each UAV state $\boldsymbol{x}_{i,k}$ and its corresponding control sequence $\boldsymbol{U}^*_{i,k-1}$, and the measurement covariance matrix $\boldsymbol{R}_{i,k}$.

Output: Optimal control sequence $\boldsymbol{U}^*_{i,k}$.

Step 1: If $\rho_{i,k} \leqslant r_{thres}$ and circular direction is inconsistent, then compute $u_{wi,k}$ based on LVFG, reset the control sequence as Section 4.4, then terminate the algorithm.

Step 2: If $\rho_{i,k} > r_{thres}$ or circular direction is consistent, initialize the control sequence as Section 4.3.

Step 3: Extrapolate target state $\boldsymbol{x}_{Fi,l}$ and UAV state $\boldsymbol{x}_{j,l}$ according to target and UAV dynamic models, where $l = k, \ldots, k+N_r$, $j \in N$.

Step 4: Calculate Lagrange multipliers $\boldsymbol{\lambda}_l$ by Eqs. (19) and (20), $l = k+1, \ldots, k+N_r$, and gradient $\dfrac{\partial H^{\mathrm{T}}_{i,l}}{\partial \boldsymbol{u}_{i,l}}$ by Eq. (31), $l = k, \ldots, k+N_r-1$.

Step 5: Calculate performance function by Eq. (10).

Step 6: If performance function decreases, then execute iterative optimization step by Eq. (34), otherwise, reduce the iterative step length.

Step 7: If the iterative step length is less than the termination threshold, terminate the algorithm, otherwise, go to Step 3.

east at cruising speed of $20\,\mathrm{m}\cdot\mathrm{s}^{-1}$ with a maximum speed variation $\Delta v_{\max} = 5\,\mathrm{m}\cdot\mathrm{s}^{-1}$ and a maximum turning rate of $\omega_{\max} = 30^\circ\cdot\mathrm{s}^{-1}$. In addition, we assumed a target moving at a constant speed with initial position (2000, 400) m and a velocity of (4, 3) $\mathrm{m}\cdot\mathrm{s}^{-1}$. In the simulation, each UAV is equipped with radar sensors to measure the bearing and radial distances between UAVs and the target for localization and tracking. The standard deviations of bearing and radial distance measurement noise are $\sigma_\beta = 1^\circ$ and $\sigma_\rho = 60\,\mathrm{m}$, respectively. The sampling time is $T_s = 0.5\,\mathrm{s}$. For implementing the proposed method, the length of the receding horizon is set as $N_r = 9$ (equivalent to 4.5 s) to ensure that the UAVs have sufficient time to predict possible turns. The initial optimization step $\Delta^0_{i,k}$ was set to 0.02 and the iteration termination threshold was $\varepsilon = 0.001$. The above simulation parameters are listed in Table 1. The circular motion direction of multiple UAVs is consistently determined by the first UAV arriving at the standoff circle.

5.1 Comparison with different methods

The proposed method is compared with LVFG-based multiple UAV standoff tracking. The simulation results from a single run are shown in Figs. 3–7. The UAV trajectories obtained from the evaluated control methods are shown in Fig. 3, along with target tracking filter results and the standoff circle at the last moment,

Table 1 Simulation parameters.

Parameter	Value	Unit
Target initial position	(2000, 400)	m
Target initial velocity	(4, 3)	$\mathrm{m}\cdot\mathrm{s}^{-1}$
$\Delta v_{\max}$	5	$\mathrm{m}\cdot\mathrm{s}^{-1}$
$\omega_{\max}$	30	$^\circ\cdot\mathrm{s}^{-1}$
σ_β	1	$^\circ$
σ_ρ	60	m
T_s	0.5	s
N_r	9	N/A
$\Delta^0_{i,k}$	0.02	N/A
ε	0.001	N/A

Note: N/A denotes not applicable.

whereas Fig. 3b shows the trajectories of the UAVs relative to the real target position. Figures 4–7 present control commands, the radial distance between UAVs and target, the phase difference between UAVs and CRLB versus time, respectively, where CRLB curves are calculated with the real target position and resulting trajectories of different methods.

As shown in Fig. 3, the resulting trajectories of different methods can approach the target and achieve

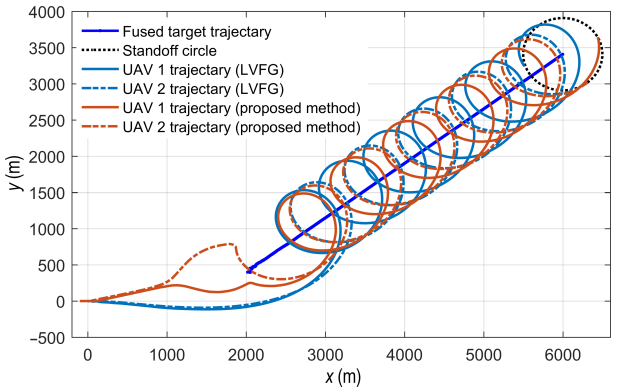

(a) Resulting trajectories and standoff circle at last moment

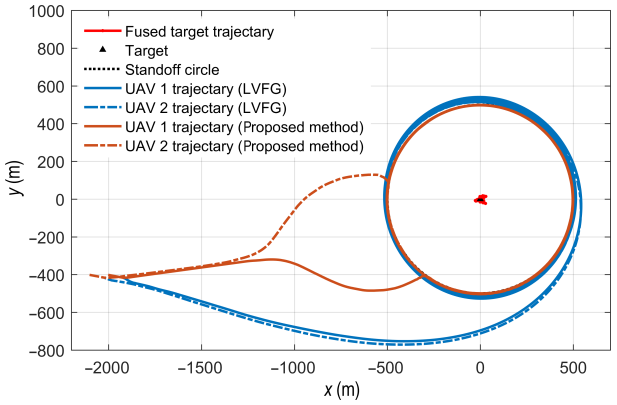

(b) Resulting trajectories relative to real target

Fig. 3 UAV trajectories and target estimate results, where x and y denote the horizontal and vertical positions, respectively.

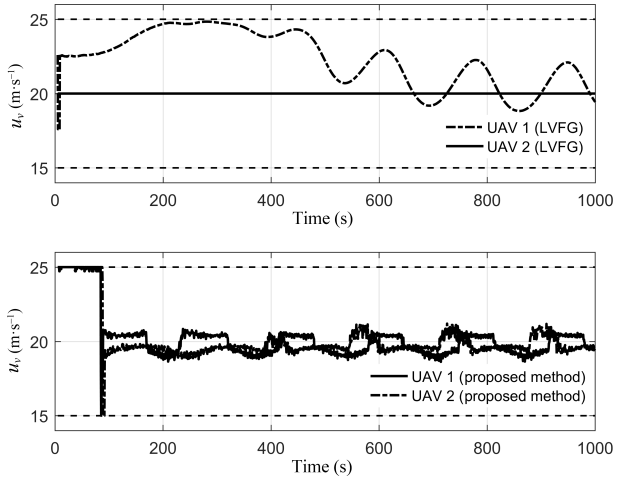

(a) Speed control command of UAVs

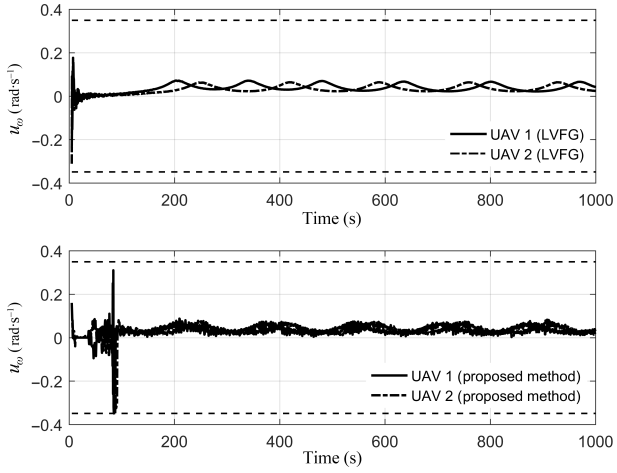

(b) Turning rate control command of UAVs

Fig. 4 Control commands of different methods versus time.

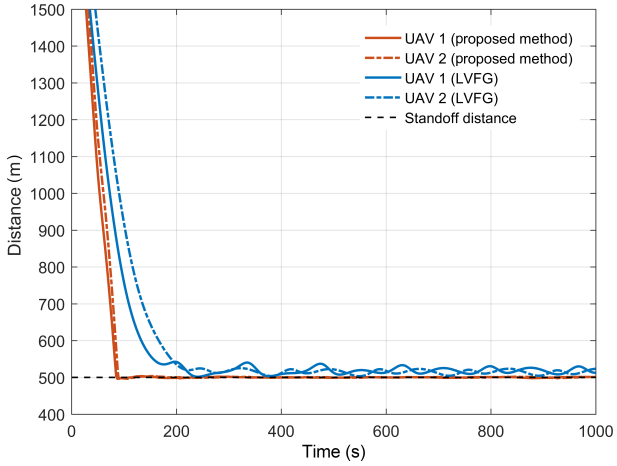

Fig. 5 Distance between UAVs and target versus time.

standoff target tracking from their initial positions. Although the control commands of the LVFG-based method are smoother because of its decoupling, as shown in Fig. 4, the difference in sensor performance leads to poor observation. For the proposed method driven by observation, UAVs tend to approach the target at the maximum speed with the expansion of phase separation. Therefore, target localization can be greatly promoted in the initial tracking stage, although the control commands are fluctuating in a small range. Some factors may lead to fluctuation, such as target state estimate error and convergence accuracy of the control commands caused by a large optimization step or early iteration termination. In flight control system, the fluctuation can be weakened by reducing the step or increasing the number of iterations, even introducing some control signal filters. After quickly arriving at the standoff circle, UAVs have better distance and phase keeping, as shown in Figs. 5 and 6, considering the prediction of the target state. $\Delta\beta_k$ is the phrase difference from the two UAVs to the target. These advantages achieve better CRLB with the proposed method, as shown in Fig. 7.

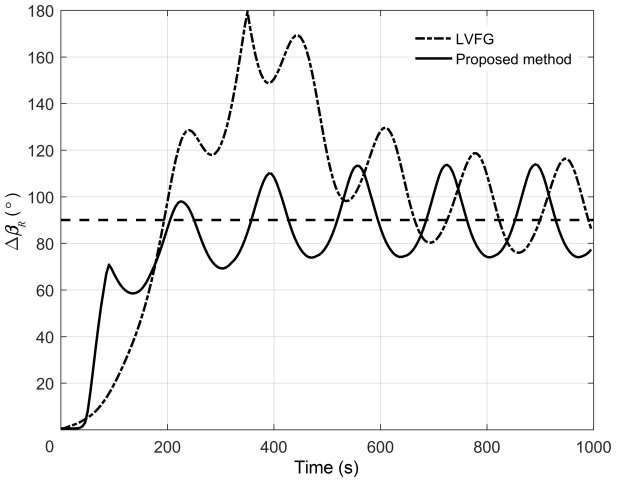

Fig. 6 Phase difference between UAVs versus time.

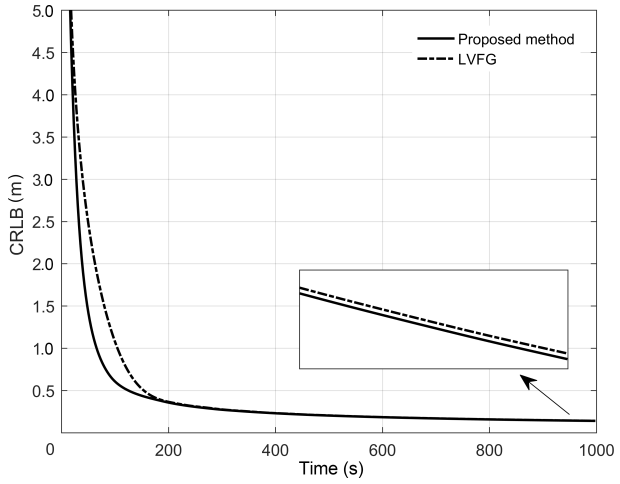

Fig. 7 CRLB curves of different methods versus time.

To further demonstrate the advantage of the proposed

Table 2 Performance evaluation of different algorithms.

Algorithm		C_S (m·s^{-1})	C_T (rad·s^{-1})	Arrival time (s)	Average of DE (m)	Average of PDE (°)	Elapsed time (s)
LVFG	UAV 1	2510.0	37.4	216.12	17.96	0.51	**5.69**
	UAV 2	**0**	**32.6**	204.49	15.06	0.51	**5.69**
Proposed method	UAV 1	**944.5**	**36.5**	**84.18**	**0.67**	**0.23**	58.31
	UAV 2	887.0	37.6	**87.97**	**0.75**	**0.23**	58.31

method, 100 Monte Carlo simulations are executed to evaluate control consumptions, arrival time, stable tracking performance, and elapsed time. The specific results are listed in Table 2, where control consumptions of speed (C_S) and turning rate (C_T) are computed with the time integration of $|u_{vi,k} - v_c|$ and $|u_{\omega i,k}|$ during the entire tracking, stable tracking performance is measured by the average of Distance Error (DE) $|\rho_k - r_d|$ and Phrase Difference Error (PDE) $|\Delta\beta_k - 90|$ after arrival time, and the time when $|\rho_k - r_d|$ is first less than 5% r_d is defined as the arrival time. The Root Mean Square Error (RMSE) of target localization is presented in Fig. 8.

LVFG-based multiple UAVs standoff tracking and its phase control are achieved by decoupling the heading control from the speed control, which significantly reduces computation time and results in low target localization performance. In contrast, by optimizing control, the proposed MPC-based method obtains the optimization direction for control using the performance function describing observation. Although control commands are coupled and the elapsed time is long, the proposed method has the advantages of stable tracking performance and arrival time with comparative control consumptions. The RMSE of target localization significantly improves between 60 s and 200 s, benefiting from the observation improvement between 20 s and 250 s, as shown in Fig. 7.

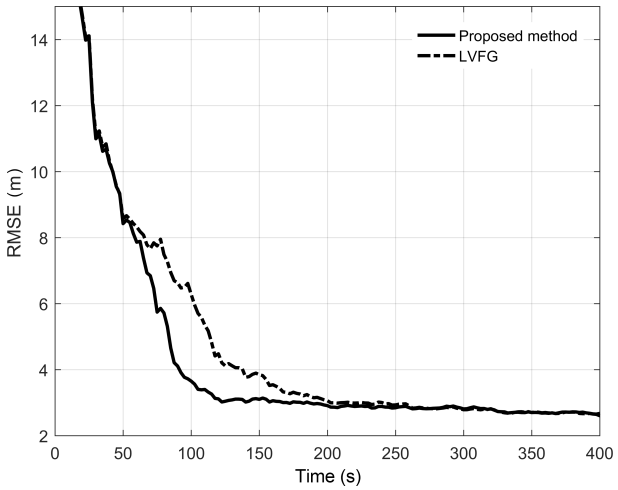

Fig. 8 RMSE of target localization versus time.

5.2 Performance under different conditions

The performance of the proposed method with different sensor performance, initial conditions, and numbers of UAVs is further evaluated. The UAV trajectory results under different measurement standard deviations of radial distance and bearing are shown in Fig. 9. The circular directions are different under different conditions; however, the two UAVs have consistent directions benefiting from the consistent control shown in Section 4.4.

When the noise of radial distance is low (bearing noise is large), corresponding closely to the pure ranging, the two UAVs first separate and increase the phase separation to triangulate the target, and then fly close to the target while maintaining a 90° phase difference. As the noise of distance measurement increases (bearing noise decreases), the resulting trajectories begin to trade off separation and approach the target. When σ_ρ=60 m in Fig. 9 (σ_β=0.5° in Fig. 10), the UAVs prioritize toward the goal and then increase the phase difference. Furthermore, when σ_ρ is large (σ_β is small), the observation system closely corresponds to the bearing-only system. The UAV trajectories tend to balance the radial and tangential velocity components. Because of the poor observability of gathering UAVs for the target, phase separation needs to increase more urgently to improve their observability as σ_ρ increases

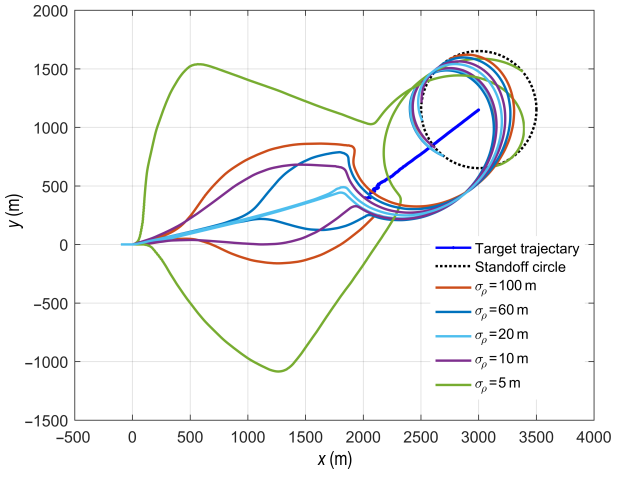

Fig. 9 UAV trajectories under different radial distance measurement errors (σ_β =1°).

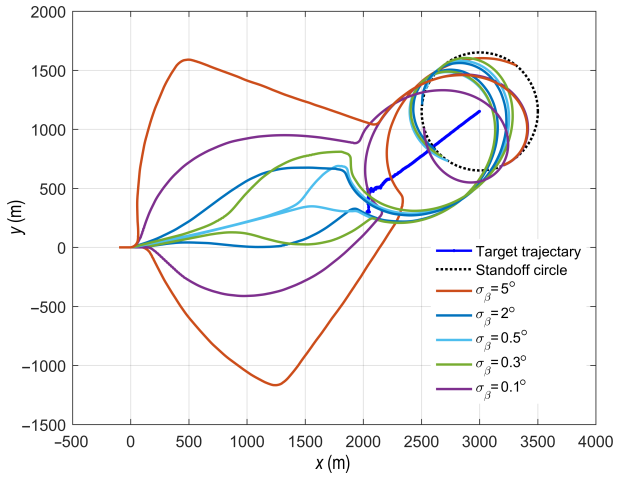

Fig. 10 UAV trajectories under different bearing measurement errors (σ_ρ=20 m).

(σ_β decreases), which means a larger tangential velocity component. However, the tangential velocity will not be significantly larger than the radial velocity like pure ranging.

When the initial distance between the UAV and the target is different, the UAV trajectory results are present in Fig. 11, where the target is fixed at (4500, 0) m, and the initial horizontal positions of the first UAV are 0 m, 1000 m, 2000 m, 2500 m, and 3000 m. Driven by the improvement in the observation capability, UAVs try to arrive on the standoff circle more directly when they are close to the target, whereas UAVs tend to increase the phase separation first because the bearing measurement has poor localization for the remote target, so UAVs separate to improve observation as pure ranging.

A nondimensional parameter[18] is defined as $\sigma=\dfrac{\rho\sigma_\beta}{\sigma_\rho}$,

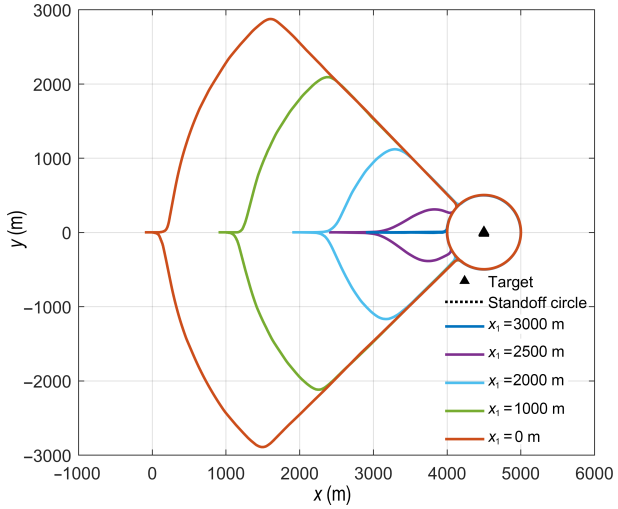

Fig. 11 Different initial distances between the UAV and the target (σ_ρ=7 m, σ_β=1°).

where ρ denotes the distance between the UAV and the target. As parameter σ becomes smaller, the observation system goes from closing pure ranging to range-bearing, then to bearing-only. The tendencies of the corresponding UAV trajectories are separation first, a tradeoff between separation and approaching, approaching target first, and a tradeoff between them again. UAV trajectories remain unchanged if standard deviations of distance and bearing measurements proportionally change, such as UAV trajectories with σ_ρ=10 m in Fig. 10 and σ_β=2° in Fig. 11, except for tiny variations caused by errors of target state estimates because of measurement noise.

The trajectory results using different numbers of UAVs are shown in Fig. 12, and the corresponding CRLB curves are presented in Fig. 13. Three UAVs separate first; then adjacent UAVs maintain a phase difference of 60° to approach the target and perform steady tracking. For four UAVs, the UAVs are divided into two equal teams and approach the target with phase separation of 90° between the teams. When five UAVs perform standoff tracking, UAVs split into three teams of 2, 1, and 2, and approximately maintain 60° to arrive on the circular orbit. When four or five UAVs are on the standoff circle, the maximum phase difference is between 125° and 180°. The phase separations of adjacent UAVs are non-uniform, presumably because the observation performance function is relatively flat. Specifically, the contribution of the phase separations to observation may be weak.

As shown in Fig. 13, the observation capability during the entire tracking process can be improved with more UAVs; however, the improvement gradually decreases. Compared with two UAVs, the addition of a third UAV can improve CRLB by 16.93%. Adding the fourth UAV improves by 13.74%, and the fifth additional UAV only improves by 11.38%. Thus, the formation with two or three UAVs is a common solution for target localization and tracking, balancing between efficiency and tracking performance.

Table 3 lists the Average Elapsed Time (AET) at the different steps of the proposed algorithm on a single UAV. Benefiting from the advantage of the decentralized control architecture, as the number of UAVs increases, the total AET increases slowly. Although the calculations of gradient and performance function consume the most time because of multiple iterations, derivation, and vectorization, there is still plenty of room to optimize code execution efficiency.

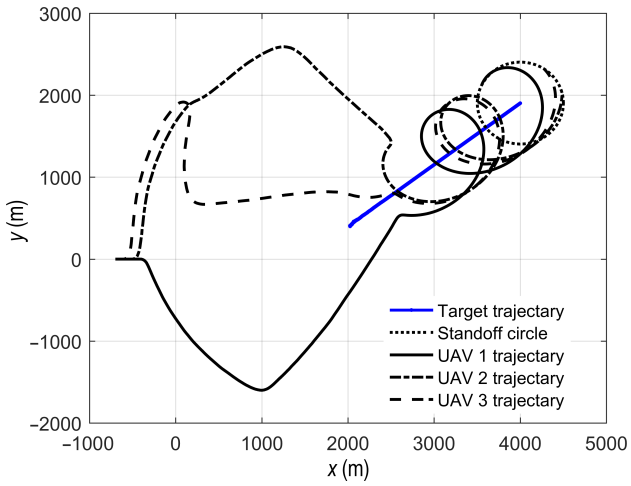

(a) Three UAVs

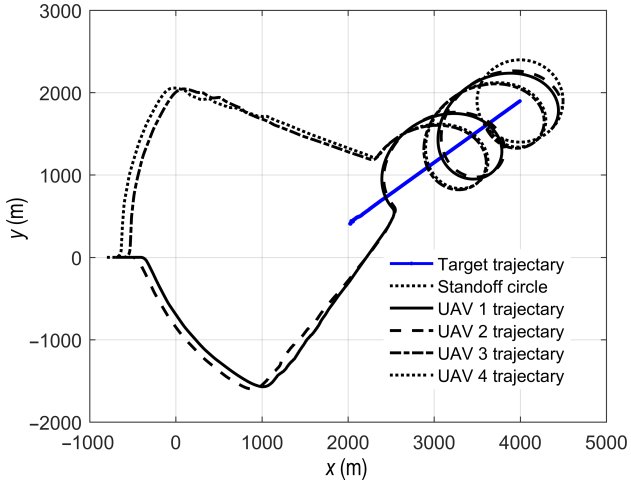

(b) Four UAVs

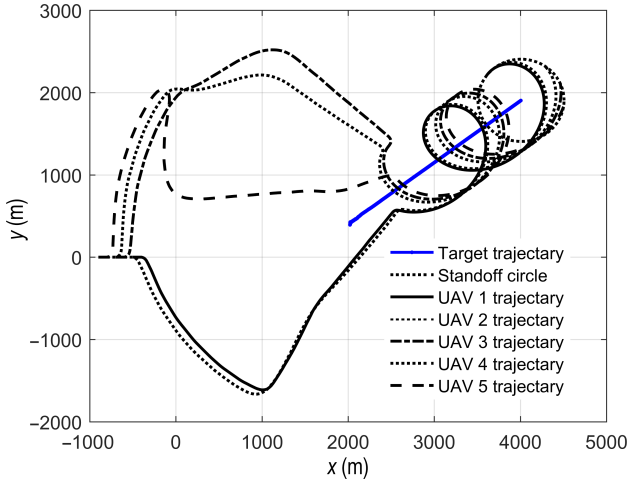

(c) Five UAVs

Fig. 12 Trajectory results with different numbers of UAVs.

The maximum elapsed time of a single run is also listed in Table 3, and it is no greater than 200 ms, which indicates the proposed method is a real-time method.

An iterations histogram with/without gradient normalization is shown in Fig. 14, where capital L stands for consistent circular direction control and simulation time is 1000 s.

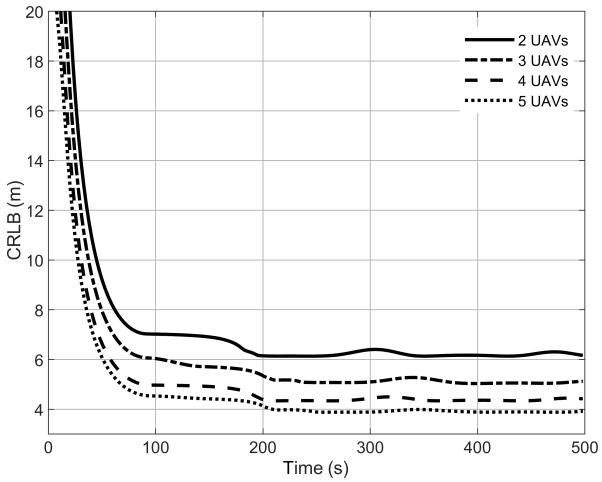

Fig. 13 CRLB with different numbers of UAVs.

For visual presentation, the frequency axis is set to logarithmic scaling. Figure 14 indicates the frequency components mainly concentrate on 5–9 iterations with gradient normalization, and frequency with an iteration number no less than 13 is 62 times. Without gradient normalization, an iteration number greater than 9 times is more frequent. Moreover, the frequency with an iteration number no less than 13 achieves 295 times, which is nearly 5 times as large as the proposed method. The proposed gradient normalization can reduce the number of iterations and significantly improve the convergence efficiency of the proposed method. Additionally, there is no impact between the consistent circular direction control and gradient normalization.

5.3 Verification with the real ground vehicle trajectory

To further verify the practicability of the proposed method, noisy measurements are generated with real trajectory data points of a ground vehicle selected from the GeoLife GPS Trajectories dataset[25, 26], which is displayed in Fig. 15 with Google geographic satellite data overlaid.

This GPS trajectory dataset was collected in the (Microsoft Research Asia) GeoLife project by 182 users in a period of over three years. The selected continuous trajectory data contains 853 time-sampled points with a total distance of approximately 42.4 km and a total duration of 68 minutes, which records a ground vehicle route from pickup to the airport at midnight in Beijing, May 21, 2009. The main difficulty of real trajectory data

Table 3 AET at different steps of the proposed algorithm.

(ms)

Number of UAVs	Target state extrapolation	UAV state extrapolation	Gradient calculation	Performance function calculation	Control iteration	Total AET	Maximum single run time
2	0.06	0.47	9.61	5.66	0.04	15.83	73.05
3	0.06	0.46	11.23	7.16	0.04	18.95	71.38
4	0.06	0.47	12.39	8.44	0.03	21.39	92.05
5	0.06	0.49	14.07	10.04	0.04	24.70	130.55

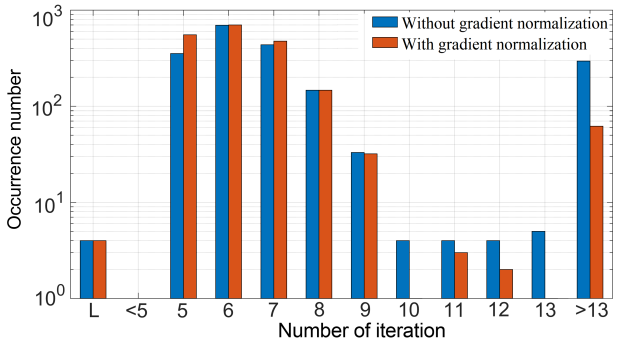

Fig. 14 Iteration histogram with/without gradient normalization.

is twofold. On the one hand, the trajectory data have a slight disturbance in the low sampling rates (every 2–5 s per point), and 94% of the trajectory is 5 s per point. On the other hand, the car target on the traffic includes the maneuver of steering, brake, and acceleration according to traffic jams and signal lamps.

To address the stop-and-go target tracking, a maneuvering target tracking based on the Singer model[27, 28] was introduced to adapt to the strong maneuvering change of the target. Similarly, the corresponding target state transfer matrix and process noise covariance matrix were modified[27], where the maneuvering time constant is set to 0.9, and the initial covariance of the target state estimate is set as $\boldsymbol{P}_t = \text{diag}(10^5, 10^3, 10, 10^5, 10^3, 10)$. The target tracking based on the Singer model is a mature technology, and a detailed model is not provided given space limitations. The noise standard deviations of bearing and radial distance measurements are 1° and 10 m, respectively. The initial positions of the first UAV and ground vehicle are set as (2000, 0) m and (0, 0) m, respectively. The other conditions remain unchanged. UAVs trajectory results and some details using different methods are presented in Fig. 16, followed by the corresponding distance curves between UAVs and the target in Fig. 17, where critical road conditions and the target maneuver are labeled. The improved performance is measured with a CRLB ratio of LVFG for the proposed method. The larger CRLB ratio implies the improvement of the observation capability of the UAV system. The CRLB ratio is also plotted in Fig. 17, and its y-axis is shown on the right side to clearly demonstrate its change with the target motion.

Although the ground vehicle target presents frequent strong maneuvers because of traffic and road conditions, the vehicle can be tracked by the target state estimator

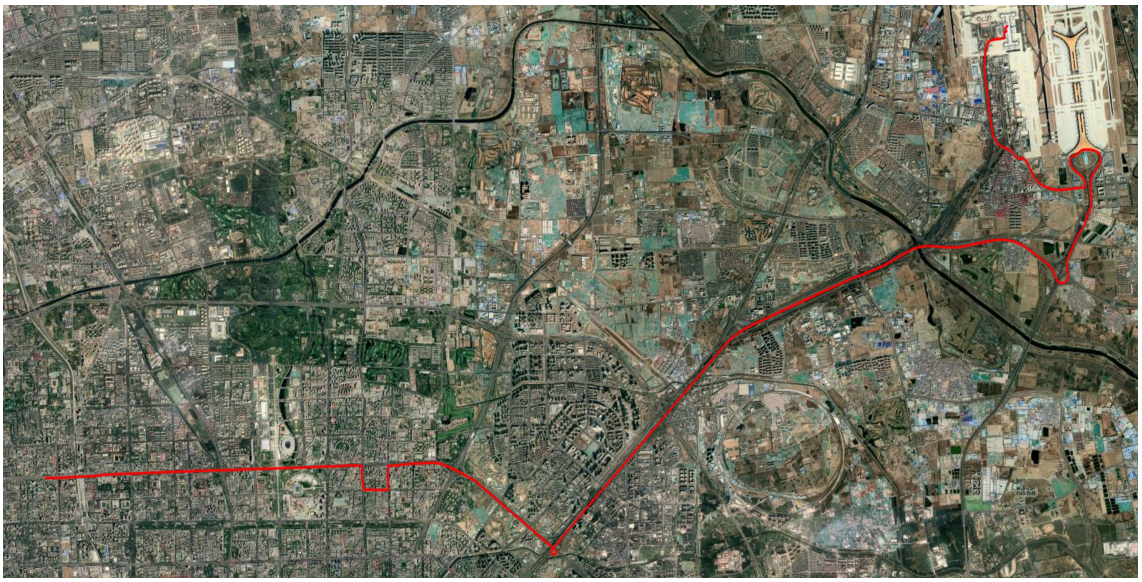

Fig. 15 Ground vehicle trajectory on a road of Beijing with geographic satellite data overlaid.

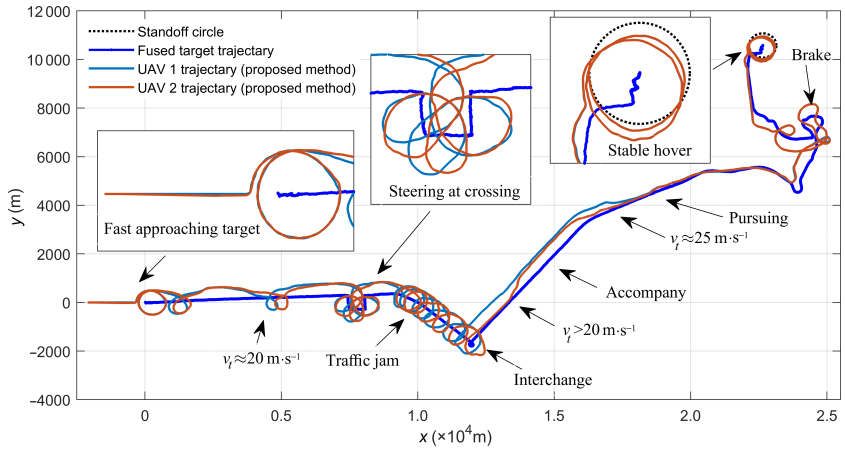

(a) LVFG method

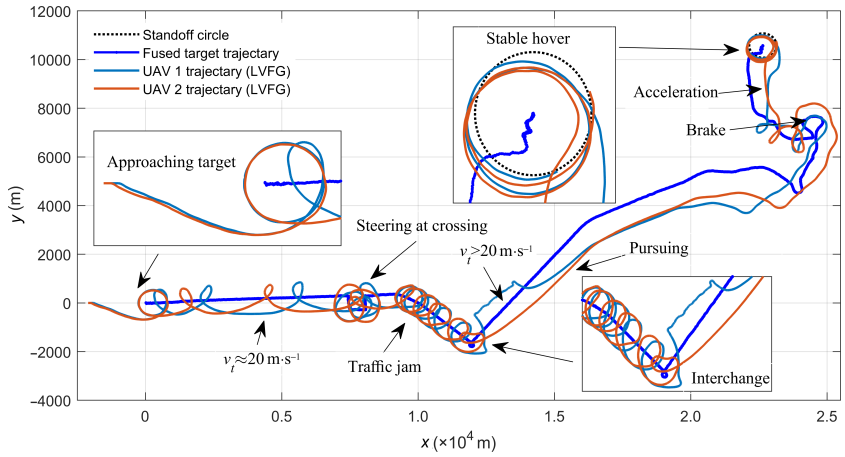

(b) Proposed method

Fig. 16 Resulting trajectories with generated noisy measurements.

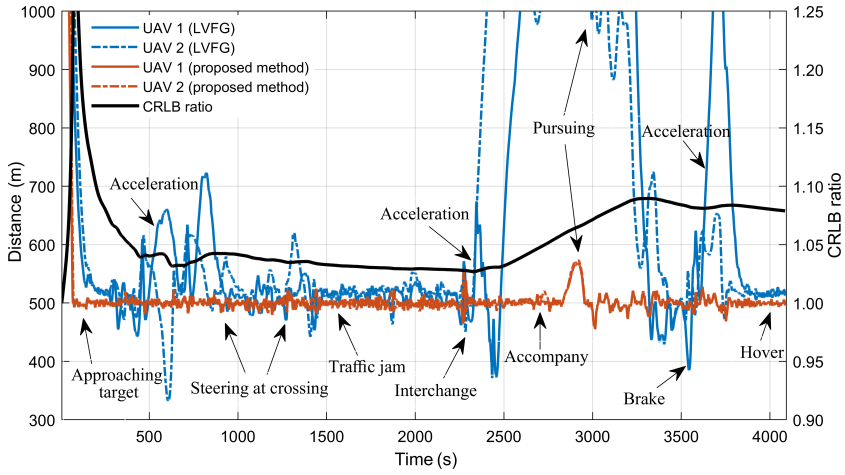

Fig. 17 Distance between UAVs and target, CRLB ratio, and target motion label.

based on the Singer model, and the UAV can perform standoff tracking for the fuzed target position estimate. When the target runs at low speed, i.e., steering at the crossing or crawling because of road congestion, the two methods all perform well by maintaining a stable distance. However, when the ground vehicle speeds up and drives close to or faster than the cruising speed of the UAV, the LVFG method causes the UAVs to fall behind the target. The decoupling control scheme limits the speed control input range of the first UAV

and slows convergence of the vector field to the standoff circle[4], which results in frequently pursuing the target and increasing the CRLB ratio that is most obvious between approximately 2350 s and 3300 s. Alternatively, the proposed observation-driven method maintains a stable distance with the target, despite the high speed of the target, which makes the CRLB ratio greater than 1. When the target speed is approximately equal to the maximum speed of the UAV, UAVs pursue the target via an accompanying flight because of the abrupt acceleration of the ground vehicle. The proposed method also performs well in the process of approaching target at the initial stage and pursuing stage. Specifically, the experiment with the real trajectory further illustrates the proposed method is effective and practical.

6 Conclusion

(1) An observation-driven multiple UAV coordinated standoff tracking is proposed to optimize trajectories of UAVs and achieves optimal observation improvement during the approach to or loitering over a moving target. Moreover, the method can be further extended to multiple target tracking with the addition of target programming.

(2) Under the effect of sensor performance and UAV-target geometry on target localization and tracking, a novel performance function is proposed with the determinant of the FIM to improve target observation in the decentralized architecture. Moreover, an optimization scheme is designed to meet saturation constraints for heading and speed control without weighted penalty functions that may impact the optimization direction.

(3) A modified iterative process accelerates the convergence and iteration speed, and consistent circular direction control guarantees stable observation in the long term.

(4) Results from sufficient simulations and real ground vehicle trajectory verify that the proposed method is real-time and adaptive for different numbers of UAVs, sensors performance, and geometries between the UAVs. The UAV trajectories can also be effectively optimized to achieve stable standoff target tracking and high observation performance.

Acknowledgment

The authors give their sincere thanks to the editors and the anonymous reviewers for their constructive comments of the manuscripts. This work was supported in part by the National Natural Science Foundation of China (Nos. 62022092 and 61790550).

References

[1] M. R. Khosravi and S. Samadi, Mobile multimedia computing in cyber-physical surveillance services through UAV-borne Video-SAR: A taxonomy of intelligent data processing for IoMT-enabled radar sensor networks, *Tsinghua Science and Technology*, vol. 27, no. 2, pp. 288–302, 2022.

[2] D. A. Lawrence, Lyapunov vector fields for UAV flock coordination, in *Proc. 2nd AIAA "Unmanned Unlimited" Systems, Technologies, and Operations Conf.*, San Diego, CA, USA, 2003, pp. 1–8.

[3] A. A. Pothen and A. Ratnoo, Curvature-constrained Lyapunov vector field for standoff target tracking, *J. Guid., Control, Dyn.*, vol. 40, no. 10, pp. 2725–2735, 2017.

[4] S. Sun, H. P. Wang, J. Liu, and Y. He, Fast Lyapunov vector field guidance for standoff target tracking based on offline search, *IEEE Access*, vol. 7, pp. 124797–124808, 2019.

[5] T. H. Summers, M. R. Akella, and M. J. Mears, Coordinated standoff tracking of moving targets: Control laws and information architectures, *J. Guid., Control, Dyn.*, vol. 32, no. 1, pp. 56–69, 2009.

[6] S. Lim, Y. Kim, D. Lee, and H. Bang, Standoff target tracking using a vector field for multiple unmanned aircrafts, *J. Intell. Robot. Syst.*, vol. 69, nos. 1–4, pp. 347–360, 2013.

[7] H. Oh, S. Kim, H. S. Shin, and A. Tsourdos, Coordinated standoff tracking of moving target groups using multiple UAVs, *IEEE Trans. Aerosp. Electron. Syst.*, vol. 51, no. 2, pp. 1501–1514, 2015.

[8] F. Gavilan, R. Vazquez, and E. F. Camacho, An iterative model predictive control algorithm for UAV guidance, *IEEE Trans. Aerosp. Electron. Syst.*, vol. 51, no. 3, pp. 2406–2419, 2015.

[9] C. F. Hu, Z. L. Zhang, Y. Tao, and N. Wang, Decentralized real-time estimation and tracking for unknown ground moving target using UAVs, *IEEE Access*, vol. 7, pp. 1808–1817, 2019.

[10] C. G. Prévost, O. Thériault, A. Desbiens, É. Poulin, and E. Gagnon, Receding horizon model-based predictive control for dynamic target tracking: A comparative study, in *Proc. AIAA Guidance, Navigation, and Control Conf.*, Chicago, IL, USA, 2009, pp. 1–9.

[11] S. Kim, H. Oh, and A. Tsourdos, Nonlinear model predictive coordinated standoff tracking of a moving ground vehicle, *J. Guid., Control, Dyn.*, vol. 36, no. 2, pp. 557–566, 2013.

[12] R. Kaune and A. Charlish, Online optimization of sensor trajectories for localization using TDOA measurements, in *Proc. 16th Int. Conf. Information Fusion*, Istanbul, Turkey, 2013, pp. 484–491.

[13] S. R. Semper and J. L. Crassidis, Decentralized geolocation and optimal path planning using limited UAVs, in *Proc. 12th Int. Conf. Information Fusion*, Seattle, WA, USA, 2009, pp. 355–362.

[14] Y. Zhong, X. Y. Wu, S. C. Huang, C. J. Li, and J. F. Wu, Optimality analysis of sensor-target geometries for bearing-only passive localization in three dimensional space, *Chin. J. Electron.*, vol. 25, no. 2, pp. 391–396,

2016.

[15] L. Zhong, X. G. Gao, and X. W. Fu, Co-optimization of communication and observation for multiple UAVs in cooperative target tracking, (in Chinese), *Control Decis.*, vol. 33, no. 10, pp. 1747–1756, 2018.

[16] J. W. Hu, L. H. Xie, J. Xu, and Z. Xu, TDOA-based adaptive sensing in multi-agent cooperative target tracking, *Signal Processing*, vol. 98, pp. 186–196, 2014.

[17] Q. Zhu, R. Zhou, Z. N. Dong, and H. Li, Coordinated standoff target tracking using two UAVs with only bearing measurement, (in Chinese), *J. Beijing Univ. Aeronaut. Astronaut.*, vol. 41, no. 11, pp. 2116–2123, 2015.

[18] E. W. Frew, Sensitivity of cooperative target geolocalization to orbit coordination, *J. Guid., Control, Dyn.*, vol. 31, no. 4, pp. 1028–1040, 2008.

[19] A. N. Bishop, B. Fidan, B. D. O. Anderson, K. Doğançay, and P. N. Pathirana, Optimality analysis of sensor-target localization geometries, *Automatica*, vol. 46, no. 3, pp. 479–492, 2010.

[20] J. Ousingsawat and M. E. Campbell, Optimal cooperative reconnaissance using multiple vehicles, *J. Guid., Control, Dyn.*, vol. 30, no. 1, pp. 122–132, 2007.

[21] Y. He, J. J. Xiu, and X. Guan, *Radar Data Processing With Applications*, (in Chinese). 3rd ed. Beijing, China: Publishing House of Electronics Industry, 2013.

[22] Y. Liu, J. Liu, C. G. Xu, G. Li, and Y. He, Fully distributed variational Bayesian non-linear filter with unknown measurement noise in sensor networks, *Sci. China Inf. Sci.*, vol. 63, no. 11, p. 210202, 2020.

[23] K. L. Lu, R. Zhou, and H. Li, Event-triggered cooperative target tracking in wireless sensor networks, *Chin. J. Aeronaut.*, vol. 29, no. 5, pp. 1326–1334, 2016.

[24] Z. R. Ding, Y. Liu, J. Liu, K. M. Yu, Y. Y. You, P. L. Jing, and Y. He, Adaptive interacting multiple model algorithm based on information-weighted consensus for maneuvering target tracking, *Sensors*, vol. 18, no. 7, p. 2012, 2018.

[25] Y. Zheng, Q. N. Li, Y. K. Chen, X. Xie, and W. Y. Ma, Understanding mobility based on GPS data, in *Proc. 10^{th} Int. Conf. Ubiquitous Computing*, Seoul, Republic of Korea, 2008, pp. 312–321.

[26] Y. Zheng, L. Z. Zhang, X. Xie, and W. Y. Ma, Mining interesting locations and travel sequences from GPS trajectories, in *Proc. 18^{th} Int. Conf. World Wild Web*, Madrid, Spain, 2009, pp. 791–800.

[27] S. Y. Jia, Y. Zhang, and G. H. Wang, Highly maneuvering target tracking using multi-parameter fusion singer model, *J. Syst. Eng. Electron.*, vol. 28, no. 5, pp. 841–850, 2017.

[28] C. Wang, C. Guo, Y. Liu, and Y. He, Group tracking algorithm for split maneuvering based on complex domain topological descriptions, *Chin. J. Aeronaut.*, vol. 31, no. 1, pp. 126–136, 2018.

Shun Sun received the MS and PhD degrees in information and communication engineering from Naval Aviation University, China in 2016 and 2020, respectively. He received joint education from the College of Electronic Science, National University of Defense Technology in 2017. He is now a postdoctoral researcher at the Department of Control Science and Technology, Naval Aviation University. His current research interests include target localization and tracking, situation awareness, multi-agent collaboration, and information fusion.

Shaojun Guo received the BEng and PhD degrees in information and communication engineering from Naval Aviation University, China in 2008 and 2017, respectively. Since 2018, he has been at Academy of Military Science PLA, where he is currently a researcher. His research interests include image processing and artificial intelligence.

Xiaohu Yuan received the BEng degree in aircraft control and test engineering from Naval Aviation University, China in 2000, and the PhD degree in control science and engineering from Tsinghua University, China in 2018. He is currently a research assistant at the Department of Automation, Tsinghua University. His research interests include RL and swarm intelligence.

Yu Liu received the BEng and PhD degrees in information and communication engineering from Naval Aviation University, China in 2008 and 2014, respectively. Since 2014, he has been with the faculty of Naval Aviation University, where he is currently a professor at the Research Institute of Information Fusion. From 2016 to 2018, he was a postdoctoral researcher at the Department of Information and Communication Engineering, Beihang University, Beijing, China. From 2020 till now, he is a visiting scholar at the Department of Electronic Engineering, Tsinghua University, Beijing, China. His research interests include multi-sensor fusion, state estimation, and situation awareness.

Gang Li received the BEng and PhD degrees in electronic engineering from Tsinghua University, China in 2002 and 2007, respectively. Since July 2007, he has been working at Tsinghua University, where he is currently a professor at the Department of Electronic Engineering. From 2012 to 2014, he visited Ohio State University, Columbus, OH, USA, and Syracuse University, Syracuse, NY, USA. He has authored/coauthored more than 120 journal and conference papers. His research interests include radar imaging, distributed signal processing, sparse signal processing, micro-Doppler analysis, and information fusion. He is an associate editor for *IEEE Transactions on Signal Processing*.